

VISCOUS DRAG CALCULATIONS FOR SHIP HULL GEOMETRY

Cheng-Wen Lin ¹, Scott Percival ¹, and Eugene H. Gotimer ¹

1.0 ABSTRACT

This paper focuses on viscous drag computations based on Reynolds-averaged, Navier-Stokes (RANS) equations. Computations were performed on axisymmetric bodies of revolution at angles of attack ranging from 0 to 18 degrees. Calculations were also performed on three surface ship hullforms. The results were compared with experimental data and were found to be in good agreement.

A parametric study was performed on the sensitivity of the flow solutions to changing grid parameters. Minimum grid spacing, distance from the body to the outer grid boundary, and number of grid points were examined as parameters. The results were equally as sensitive to the number of grid points as to the minimum spacing. Extending the location of the outer boundary had a lesser effect on the result. This investigation was based on a single flow solver, *ISFLOW*, and may not be directly applicable to other RANS codes.

2.0 INTRODUCTION

Applications of computational fluid dynamics (CFD) to the maritime industry continue to grow as this advanced technology takes advantage of the increasing speed of computers. Numerical approaches have evolved to a level of accuracy which allows them to be used during the design process to predict ship resistance. Significant progress has been made in predicting flow characteristics around a given ship hull. Ship designers can use this information to improve a ship's design. However, not much effort has been dedicated to determining viscous drag, an important element in the development of a new design.

1. Design Evaluation Branch, Hydromechanics Directorate, David Taylor Model Basin, Carderock Division Naval Surface Warfare Center, Bethesda, MD USA.

Prediction of drag on a ship hull is always a challenging task for a naval architect. At the start of the design process, hull forms are developed given certain requirements. One of the major design tasks is to estimate the powering performance so that propulsion requirements can be determined. Early estimates of resistance and power are often based on simple empirical formulas derived from data for similar ships. As the design process proceeds, a more reliable approach becomes necessary to predict resistance; scale-model testing has been generally adopted for this purpose.

The accuracy of a prediction can be assessed by comparison with model-scale experimental results. Full-scale ship resistance prediction is the final goal. Although CFD methods can be used to calculate full-scale ship resistance, it is quite difficult to assess the accuracy of these results without a reasonable database of full-scale resistance. Such a database is not currently available.

It is beyond the text of this paper to consider full-scale calculations. The focus of the paper is to examine the effects of several uncertain/vague factors in CFD technology concerning grid generation: minimum grid spacing, grid distribution, and location of outer grid boundaries.

3.0 AXISYMMETRIC BODY OF REVOLUTION

3.1 Geometry

The first set of bodies studied was a systematic series of mathematically-defined bodies of revolution. Axisymmetric bodies are ideal candidates for a parametric study with their easily defined geometry, straightforward grid generation, and available experimental data.

Each body was defined by a sixth-degree polynomial [1]. Six axisymmetric bodies were generated with length-to-diameter ratios (L/D) ranging from four to ten. All six bodies were evaluated at zero angle of attack. The two bodies with a L/D of four and ten were also evaluated at angles of attack up to 18 degrees. (See Table 1.)

TABLE 1. Configurations examined for bodies of revolution.

L/D	Angle of attack						
	0°	2°	4°	6°	8°	12°	18°
4	•	•	•	•	•	•	•
5	•						
6	•						
7	•						
8	•						
10	•	•	•	•	•	•	•

3.2 Grid Parameters

A computational grid for each body was generated by a transfinite interpolation routine [2]. Three of the parameters characterizing a computational grid are total number of grid points, location of outer computational boundaries, and minimum spacing (initial spacing normal to body surface). Prior experience with RANS computations on similar geometry usually guides the determination of these parameters. The intent of this study is to qualify these parameters, as much as possible, and to begin to develop some guidance for their selection.

The minimum spacing is generally based on y^+ , a dimensionless parameter representing a local Reynold's number in the near-wall region. This parameter is defined as

$$y^+ \equiv \frac{yu_*}{\nu}, \quad (1)$$

where

- y = distance from wall surface,
- $u_* = \sqrt{\frac{\tau_w}{\rho}}$ frictional velocity,
- τ_w = shear stress at the wall,
- ρ = density, and
- ν = kinematic viscosity.

Using flat-plate boundary layer theory [3], this parameter can be derived as

$$y^+ = 0.172 \left(\frac{y}{L} \right) \text{Re}^{0.9}, \quad (2)$$

where

- L = body length, and
- Re = Reynold's number based on body length.

An estimate of the minimum grid spacing can be determined by setting $y^+ = 1$ and solving for the value of y/L using equation (2). It should be noted here that the y^+ value from equation (2) is based on a turbulent boundary layer on a flat plate. Therefore, it is used only as an estimate in cases where the geometry is not actually a flat plate. The actual value of y^+ for the hullform is obtained with the viscous flow solution. Furthermore, the real y^+ is not a constant but varies over the wall surface according to the flow in the boundary layer.

For the L/D and angle of attack studies, a default set of grid parameters typical for an axisymmetric body was used. In the j -direction¹ (normal to the

1. In CFD analyses of marine vehicles, it is customary to use i, j , and k to describe the grid dimensions, where the i -direction is in the axial direction, j is normal to the body, and k is around the body's girth.

body), 61 points were used. The outer boundary was located one body-length from the body and two lengths aft. A schematic of this arrangement is shown in Figure 1. The minimum spacing was based on $y^+ = 1$.

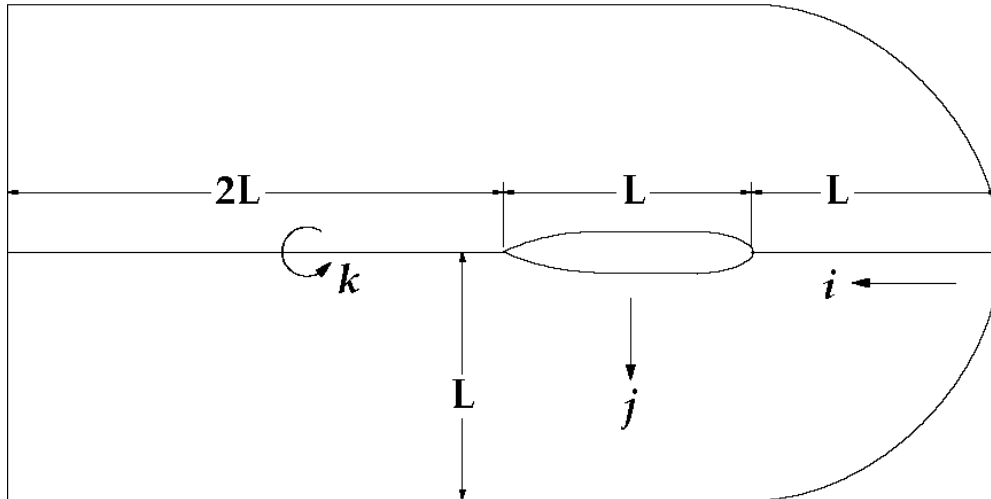


FIGURE 1. Schematic of grid structure around an axisymmetric body.

4.0 SURFACE SHIP HULLFORM

The second study examined surface ship hull-forms. The drag coefficient was computed for three ship hullforms. Generation of the geometry and grid were far more time consuming than for the bodies of revolution, due to the complex curvature of the shapes.

The first hull was the HSVA tanker, shown in Figure 2, which has been used extensively for CFD validation of the viscous flow field [4]. Detailed measurements of the viscous flow velocity field were made in a wind tunnel. By eliminating the free surface effect, the viscous drag on the double model of the HSVA tanker was measured and published in Reference [5].

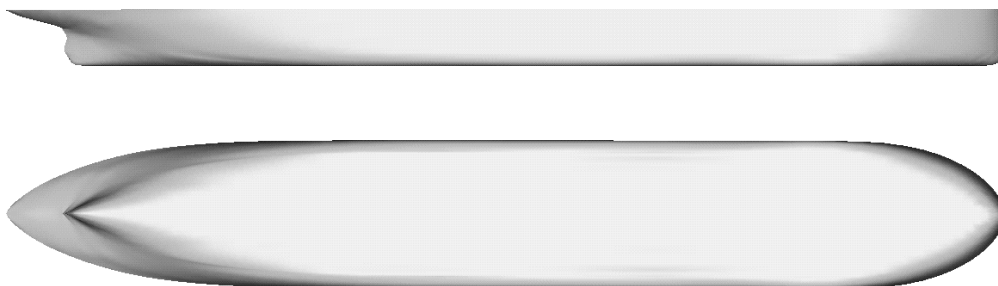
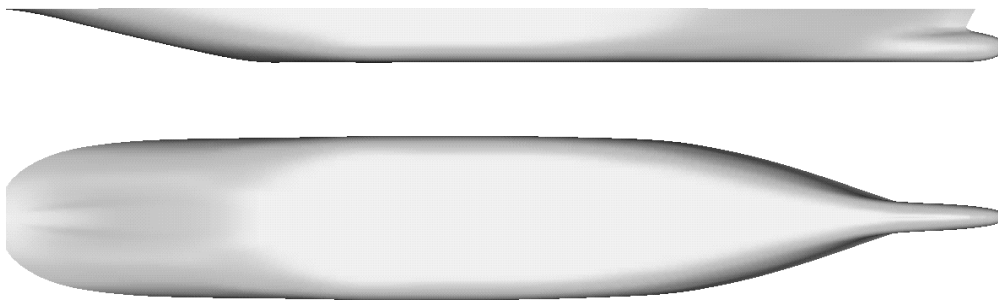


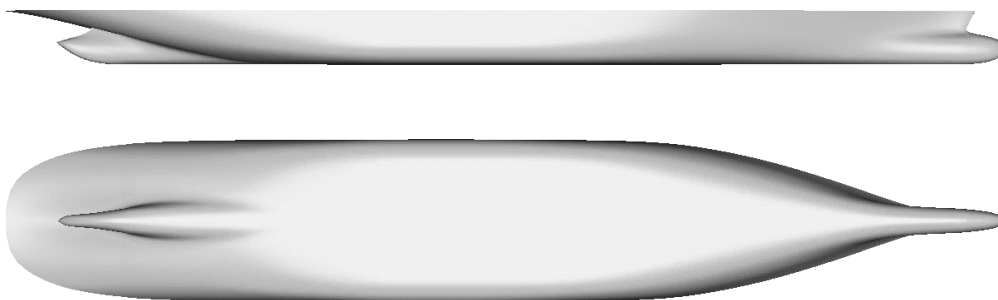
FIGURE 2. Geometry of the HSVA tanker.

A multi-block, also known as multi-zonal, structured grid was generated around the HSVA tanker with H-type grid topology. The minimum spacing was based on a y^+ of 1. Viscous flow calculations were performed to find the double body solution.

The two other ship hulls are similar to each other in shape, and differ only that the second hull has an added a centerline skeg in the stern. Figure 3 shows the two hulls. The complex curvature of these two hulls leads to a more complex grid topology than used for the HSV A tanker. The grid generation package *GRIDGEN* was used to generate the multi-block grids around the two hulls. A view of the grid structure around one of the hulls is shown in Figure 4. The minimum spacing was based on a y^+ of 1. Again, the double body solution was calculated.



a. Surface ship without a centerline skeg.



b. Surface ship with a centerline skeg.

FIGURE 3. Surface ship geometries, with and without a centerline skeg.

5.0 MULTI-ZONAL FLOW SOLVER

A multi-zonal flow solver (*ISFLOW*) has been developed for computation of multi-block structured grids. The numerical algorithm adopted was based on a cell-centered, second-order central difference, finite volume formula for spatial discretization with an explicit one-step Runge-Kutta time-stepping scheme. The three-dimensional Reynolds-averaged Navier-Stokes equations with pseudo-compressibility approach for incompressible viscous flow were written in tensor notation as follows:

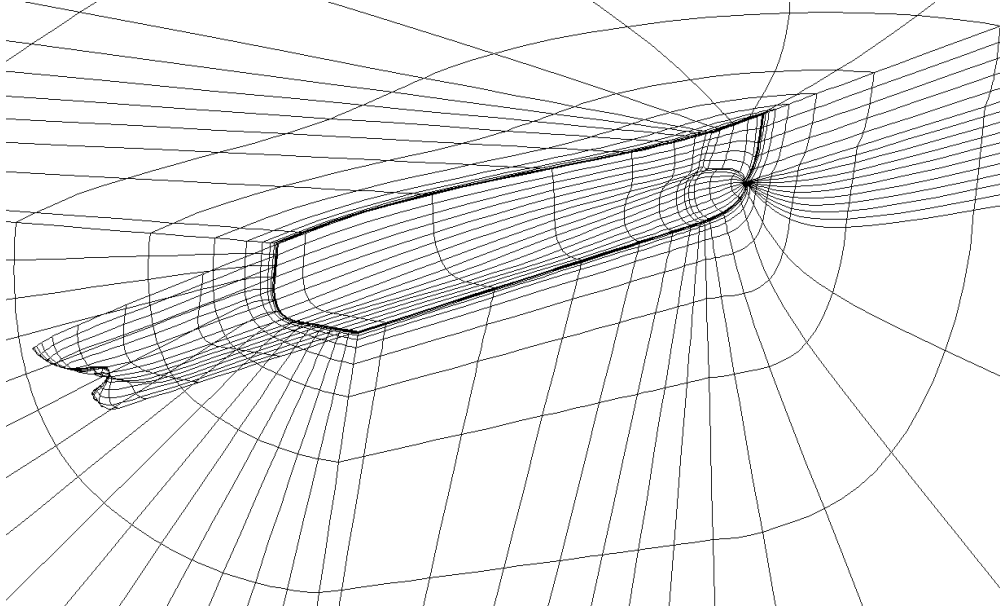


FIGURE 4. Grid structure around a surface ship.

$$\frac{1}{\beta} \frac{\partial P}{\partial t} + \frac{\partial U_i}{\partial X_i} = 0 \quad (3)$$

$$\frac{\partial U_i}{\partial t} + \frac{\partial U_i U_j}{\partial X_j} = -\frac{\partial P}{\partial X_i} + \frac{\partial \tau_{ij}}{\partial X_j} \quad (4)$$

where t represents time, X represent the Cartesian coordinates, U the corresponding velocity components, P the pressure, and τ_{ij} the viscous stress tensor. The parameter $1/\beta$ represents the pseudo-compressibility. The fact that the transient-state solution obtained by equations (3) and (4) may not be physically valid was not relevant, since only the steady-state solution was of interest here. The goal is to choose a reasonable β value in order to reduce the disparity in propagating speeds during the transient state. Numerical experiments on choosing β indicate that $\beta = 2$ gives a good convergence rate.

A combination of finite volume discretization and the Runge-Kutta time-stepping scheme was used to yield an effective method for solving equations (3) and (4) in arbitrary geometric domains. The domains are divided into quadrilateral cells. The discretization scheme decouples the approximation of the spatial and temporal terms in equations (3) and (4). In addition, the spatial terms are discretized in a finite-volume formulation. This is accomplished by defining the dependant variable at the center of a computational cell and evaluating the flux at the midpoint of each cell surface using the central differencing technique. A fourth-difference artificial dissipation was included to damp high-

frequency oscillation and stabilize the computation. Since artificial dissipation is a purely numerical parameter, which does not appear in the analytic form of the equation, it must vanish as the discrete equations approach the analytic form of equations (a limitation of the mesh refinements). In addition, the terms must vanish if a natural dissipation mechanism, such as viscosity, is strong enough to stabilize the computation. To avoid the interference of artificial damping terms with the physical transport phenomena, a hyper-tangent distribution of a weighting function for reducing the magnitude of the artificial dissipation is used for computations inside the viscous layer. The use of such a dissipation model has proved to be successful in the calculation of turbulent vortex flow around the juncture of an airfoil attached to a flat plate [6].

The discretization procedure on spatial terms in equations (3) and (4) leads to a set of coupled ordinary differential equations, which has the form

$$\frac{\partial W}{\partial t} = R(W) \quad (5)$$

where W is the vector of the flow variables and $R(W)$ is the vector of the residuals, consisting of the flux balance from the convective and diffusive terms, as well as the artificial dissipation terms. The time integration is performed by using an explicit one-step multi-stage scheme derived from a generalization of the Runge-Kutta formulation [7]. The multi-stage scheme of the Runge-Kutta method can be tailored to give the desired stability properties. The Courant-Friedrichs-Lewy (CFL) number applies a conditional stability requirement on the time step for the numerical solution. It has been determined that the maximum stability bound on the CFL number for an m -stage scheme is $(m-1)$ along the imaginary axis. The optimal choice of the scheme depends on a trade-off between the extent of the stability region needed and the cost of the integration of an extra stage. An implicit residual smoothing technique was implemented to relax the restriction on the time step imposed by the CFL condition. To accelerate the numerical solution to a steady-state, local time-stepping has also been adopted. The CFL number is increased from 3.0 to 4.5 when the 4-stage Runge-Kutta scheme is used with 2 evaluations of implicit residual smoothing. In addition, the algebraic turbulence model proposed by Baldwin and Lomax [8] for separated turbulent flows is used.

The multi-zonal capability in *ISFLOW* was designed specifically for the non-overlapping grid structure [9]. This multi-zonal approach allows the user to divide the whole flow field into a number of smaller regions. By defining these regions in a logical manner, the coding of the flow solver can be greatly simplified. In addition, a different set of governing equations and boundary conditions can be used independently within each zone. The grid distribution can also vary between zones, depending on the desired resolution.

Compared to the single zone approach, the multi-zonal approach has played a significant role in computing the flow around complicated geometry. Besides the substantial advantage for grid generation, a significant saving in

computer memory and cpu time can be achieved. The treatment of the interface boundary between neighboring zones is also important. Generally, the interior points of each zone are updated using the regular integration method similar to the single zone scheme. The interface boundary points are updated through the interpolation between interior points of neighboring zones. It is important to make the zonal boundary scheme conservative enough so that a distortion-free flow movement is achieved across the zonal interface.

6.0 RESULTS AND ANALYSIS

6.1 Axisymmetric Body of Revolution

6.1.1 Without Angle of Attack

The computed results for the six axisymmetric bodies are shown in Table 2. The total drag coefficient (C_D) is composed of viscous pressure (C_{vp}), and frictional drag (C_f), which are obtained by integrating the pressure distribution and viscous shear stress, respectively, over the body surface. The computed results are in agreement with the experimental measurements. The calculations and experiments were performed for a Reynold's number of 2.0×10^7 .

TABLE 2. Computational versus experimental results for bodies of revolution at zero angle of attack.

L/D	ISFLOW results ($\times 10^{-3}$)			Experiment ($\times 10^{-3}$)	% difference
	C_{vp}	C_f	C_D	C_D	
4	0.746	2.467	3.213	3.208	0.2
5	0.431	2.517	2.948	2.988	1.3
6	0.354	2.504	2.858	2.848	0.4
7	0.257	2.504	2.761	2.758	0.1
8	0.199	2.492	2.691	2.718	1.0
10	0.132	2.497	2.629	2.703	2.7

Several prediction methods have been investigated to calculate the drag for this series of bodies [10]. Table 3 provides a comparison of the current results with two methods in Reference [11], one based on a differential boundary layer formulation (theory of Cebeci and Smith) and the other based on a simple drag formula by White [10]. Although not as close as the RANS prediction, the two methods show good correlation with experimental data.

6.1.2 With Angle of Attack

The computed results for the two axisymmetric bodies at angles of attack are shown in Tables 4 and 5. The only experimental data available was the coefficient of force normal to the body axis (C_N) in the $y = 0$ plane. Drag (C_D), lift (C_L), and normal force (C_N) coefficients from ISFLOW were tabulated with

experimental data. For the slender body ($L/D = 10$), the computed normal forces show reasonable correlation, within 5% to 8% of the experimental val-

TABLE 3. Drag coefficients ($C_D \times 10^{-3}$) from different prediction methods.

L/D	White's formula	Boundary layer theory	ISFLOW	Experiment
4	3.108	3.028	3.213	3.208
5	2.998	2.958	2.948	2.988
6	2.928	2.898	2.858	2.848
7	2.858	2.858	2.761	2.758
8	2.808	2.818	2.691	2.718
10	2.738	2.778	2.629	2.703

ues. The fat body ($L/D = 4$) shows slightly better correlation at angles of attack up to 12 degrees, within 1% to 6% of the experiment. However, at 18 degrees the discrepancy is 13.5%.

TABLE 4. Results for the slender body ($L/D = 10$) at angles of attack.

Angle of attack	ISFLOW results ($\times 10^{-3}$)			Experiment ($\times 10^{-3}$)	% difference
	C_D	C_L	C_N	C_N	
2	2.54	0.10	0.19	0.20	5.0
4	2.48	0.26	0.43	0.41	4.9
6	2.47	0.52	0.78	0.72	8.3
8	2.52	0.93	1.27	1.20	5.8
12	2.67	2.17	2.68	2.49	7.6
18	2.95	4.95	5.62	5.20	8.1

TABLE 5. Results for the fat body ($L/D = 4$) at angles of attack.

Angle of attack	ISFLOW results ($\times 10^{-3}$)			Experiment ($\times 10^{-3}$)	% difference
	C_D	C_L	C_N	C_N	
2	3.12	0.81	0.92	0.87	5.7
4	3.15	1.63	1.85	1.74	6.3
6	3.29	2.54	2.87	2.83	1.4
8	3.58	3.57	4.03	3.98	1.3
12	4.57	6.27	7.08	7.30	3.0
18	7.39	13.10	14.74	17.05	13.5

6.1.3 Effect of Grid Parameters

The results of varying the grid parameters for the slender body at zero angle of attack are shown in Table 6. Based on equation (1), the y^+ values for the first, tenth, and twentieth cell off the body were also shown. Looking at the three $y^+(1) = 1$ cases, 61 and 71 j -points were satisfactory, but there was a loss in accuracy going from 61 to 51 j -points. Similarly, for the three 61 j -cases, values for $y^+(1)$ of 1.0 and 0.5 were satisfactory, but 2.0 has a much larger error.

TABLE 6. Effects of varying grid parameters on the solution for the slender body ($L/D = 10$) at zero angle of attack.

No. of j -points	$y^+(1)$	$y^+(10)$	$y^+(20)$	C_{vp}	C_f	C_D	Exp. $C_D = 2.703$ % diff
51	2.0	102.4	1168	0.130	2.279	2.409	10.9
	1.0	98.0	1157	0.132	2.357	2.489	7.9
	0.5	95.7	1152	0.132	2.400	2.532	6.3
61	2.0	66.0	581	0.132	2.404	2.536	6.2
	1.0	61.5	572	0.132	2.497	2.629	2.7
	0.5	59.2	567	0.134	2.538	2.672	1.1
71	1.0	42.8	337	0.135	2.540	2.675	1.0

The results of varying the grid parameters for the fat body at 18 degrees angle of attack were shown in Table 7. Both increasing the number of j -points and extending the outer boundary make small improvements in the accuracy. The reduction of y^+ has a much more significant effect in improving the accuracy of the results for these configurations.

TABLE 7. Effects of varying grid parameters on the solution for the fat body ($L/D = 4$) at 18° angle of attack.

Location of outer boundary	No. of j -points	$y^+(1)$	C_N	Exp. $C_N = 17.05$ % diff
1.25L	61	1.0	14.74	13.5
1.25L	71	1.0	14.96	12.3
1.875L	71	1.0	15.22	10.7
1.875L	71	0.5	15.88	6.9

6.2 Surface Ship

The drag calculations for the three surface ship hullforms are compared with experimental data in Table 8. Both the experiment and computations for the HSVA tanker hullform were performed for a Reynold's number of 5.0×10^6 . The computations and experiment for the other surface ships (with

and without the centerline skeg) were performed for a Reynold's number of 4.5×10^6 . A good agreement was found for the HSVA tanker and ship without the centerline skeg. However, there was a large (6.9%) difference for the ship with the centerline skeg. Consequently, the flow solution around the ship with the skeg was more thoroughly examined. A vortex along the bilge (the transition between the bottom and side of the ship) showed rapid and unusual diffusion near the ship stern. The grid spacing around the girth of the ship, especially at the bilge, is suspected to have been too large.

TABLE 8. Computational versus experimental results for surface ships.

	<i>ISFLOW</i> Results ($\times 10^{-3}$)			Experiment ($\times 10^{-3}$)	% difference
	C_f	C_{vp}	C_D	C_D	
HSVA	2.956	1.212	4.168	4.134	0.8
Ship with- out skeg	3.036	0.849	3.885	3.879	0.2
Ship with skeg	3.016	1.068	4.084	3.820	6.9

7.0 CONCLUSIONS

The lift and drag forces on both the axisymmetric bodies and the surface ships predicted by *ISFLOW* show good agreement with experimental results.

For the axisymmetric bodies at zero angle of attack a minimum spacing based on $y^+ = 1$, an outer boundary 1 body length away, and 61 j -points were sufficient to ensure good agreement with experiment. When increasing the number of grid points for a given value of y^+ , there appears to be a threshold up to which the accuracy increases rapidly, and beyond which there was little improvement.

For examining both the slender and fat bodies at low angles of attack, these grid parameters seem to be on the threshold of accuracy. The fat body clearly requires a different set of grid parameters at high angles of attack.

Overall, the results were equally as sensitive to the number of j -points as to the minimum spacing. Extending the location of the outer boundary beyond one body length has a lesser effect on the result.

8.0 REFERENCES

1. GERTLER, M - Resistance Experiments on a Systematic Series of Streamlined Bodies of Revolution For Application to the Design of High Speed Submarines, DTMB Report C-297 (1950)

2. SMITH, R E and ERIKSSON, L E - 'Algebraic Grid Generation', *Computer Methods in Applied Mechanics and Engineering* (1987)
3. SCHLICHTING, H - *Boundary Layer Theory*, McGraw-Hill, New York, (1966)
4. WIEGHARDT, K - Kinematics of Ship Wake Flow, DTNSRDC 81-093 (1982)
5. Proceedings of the CFD Workshop Tokyo (1994)
6. SUNG, C H and LIN, C W - 'Numerical Investigation on the Effect of Fairing on the Vortex Flow around Airfoil/Flat-Plate Junctionures', *AIAA 26th Aerospace Sciences Meeting* (1988)
7. JAMESON, A, SCHMIDT, W, and TURKEL, E - Numerical Solution of the Euler Equations by Finite Volume Methods Using Runge-Kutta Time Stepping Schemes, AIAA Paper 81-1259 (1981)
8. BALDWIN, B S and LOMAX, H - 'Thin Layer Approximation and Algebraic Model for Separated Turbulent Flows', *AIAA 16th Aerospace Sciences Meeting* (1978)
9. LIN, C W, SMITH, G D, and FISHER, S C - 'Numerical Viscous Flow Simulation of Wind Tunnel Model-Scaled Experiments', *The 2nd Osaka International Colloquium on Viscous Fluid Dynamics in Ship and Ocean Technology* (1991)
10. WHITE, N M - A Comparison Between a Single Drag Formula and Experimental Drag Data for Bodies of Revolution, DTNSRDC Report 77-0028 (1977)
11. WHITE, N M - A Comparison Between the Drags Predicted by Boundary-Layer Theory and Experimental Drag Data for Bodies of Revolution, DTNSRDC SPD-784-01 (1978)